FISEVIER

Contents lists available at ScienceDirect

Science of the Total Environment

journal homepage: www.elsevier.com/locate/scitotenv



Molecular and spectroscopic changes of peat-derived organic matter following photo-exposure: Effects on heteroatom composition of DOM



Mourad Harir ^{a,d,*,1}, Kaelin M. Cawley ^{b,c,1}, Norbert Hertkorn ^a, Philippe Schmitt-Kopplin ^{a,d}, Rudolf Jaffé ^{b,**}

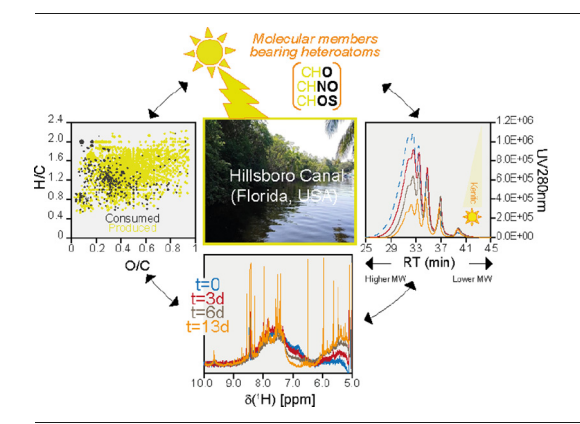
- ^a Research Unit Analytical Biogeochemistry, Helmholtz Munich, 85764 Neuherberg, Germany
- b Southeast Environmental Research Center and Department of Chemistry and Biochemistry, Florida International University, Miami, FL, USA
- ^c Battelle, National Ecological Observatory Network (NEON) Project, Boulder, CO, USA
- ^d Analytical Food Chemistry, Technische Universität München, Maximus-von-Imhof-Forum 2, 85354 Freising-Weihenstephan, Germany

HIGHLIGHTS

Photo-irradiation affects molecular and spectroscopic features of peat-derived DOM.

- Longer-term heteroatom-dependent photochemistry affects DON and DOS speciation.
- The temporal evolution of heteroatom photoproducts was non-linear.
- Ultimate fate of DON and DOS compounds is strongly driven by photochemistry.

GRAPHICAL ABSTRACT



ARTICLE INFO

Editor: Shuzhen Zhang

Keywords: DOM photo-evolution Heteroatom DOM EEM-PARAFAC FT-ICR-MS NMR

ABSTRACT

The temporal evolution of molecular compositions and changes in structural features of Hillsboro Canal (Florida, USA) dissolved organic matter (DOM) was studied with an emphasis on nitrogen and sulfur containing molecules, after a 13 day time-series exposure to simulated sunlight. The Hillsboro Canal drains from the ridge and slough wetland environment underlain by peat soils from the northern extent of the Greater Everglades Ecosystem. The Hillsboro Canal-DOM was characterized by combining ultrahigh-resolution mass spectrometry (FT-ICR-MS), high-field nuclear magnetic resonance spectroscopy (¹H NMR), size exclusion chromatography (SEC) with UV detection, and ultraviolet/visible (UV/vis) absorbance and excitation emission matrix (EEM) fluorescence spectroscopy. Size exclusion chromatography (SEC) demonstrated progressive depletion of higher mass molecules and a concomitant decrease of absorbance during photo-irradiation. NMR and FT-ICR-MS revealed nonlinear temporal evolution of DOM. In fact, FT-ICR-MS showed an initial depletion of supposedly chromophoric molecules often carrying major unsaturation accompanied by an uneven evolution of numbers of CHO, CHOS and CHNO compounds. While CHNO compounds continually increased throughout the entire photo-exposure time, CHO and CHOS compounds temporarily increased but declined after further light exposure. Progressive loss of highly unsaturated compounds was accompanied by production of low mass CHO and CHNO compounds with high O/C ratios. Area-normalized 1 H NMR spectra of DOM in water and of the water insoluble fraction (~5%) in methanol revealed clear distinctions between irradiated and nonirradiated samples and congruent evolution of DOM structural features during irradiation, with more uniform trends in methanolic-DOM. Photoirradiation caused initial photoproduction of oxygenated aliphatic compounds, continued

^{*} Correspondence to: M. Harir, Research Unit Analytical Biogeochemistry, Helmholtz Munich, 85764 Neuherberg, Germany.

^{**} Corresponding author.

E-mail addresses: mourad.harir@helmholtz-muenchen.de (M. Harir), jaffer@fiu.edu (R. Jaffé).

Authors M.H and K.M.C contributed equally to this work.

depletion of phenols and oxygenated aromatics, substantial change from initial natural product derived olefins to photoproduced olefins, and uneven evolution of carboxylated and alkylated benzene derivatives. This study demonstrates longer-term heteroatom-dependent photochemistry of DOM, which will affect the speciation of N and S heteroatoms, their connections to inorganic nutrients, and potentially their bioavailability.

1. Introduction

Dissolved organic matter (DOM) is ubiquitous in freshwater and coastal ecosystems and is derived from both allochthonous, i.e. external sources, such as soils and terrestrial plants, and autochthonous sources, i.e. biological activity within a water body. These two sources impart distinct molecular features (McKnight et al., 2001; Sleighter et al., 2010) that form a uniquely complex mixture of DOM molecules through an elaborate array of abiotic and biotic catchment processes (Chen and Jaffé, 2014; Mao and Li, 2019; Opsahl and Benner, 1998; Amon et al., 2001). DOM is comprised of a combination of biomolecules such as carbohydrates, pigments, lipids, polyketides, polyphenols, proteins and also includes significant proportions of breakdown products of cellulose, lignin and tannin, among others (McKnight and Aiken, 1998). As such, DOM is a major source of carbon and nutrients for food webs and the speciation of heteroatoms N and S has a critical control on nutrient bioavailability. Due to its high molecular diversity and the variable extent of abiotic and microbial processing, a precise understanding of molecular features of the DOM pool is challenging (Hertkorn et al., 2016; Leyva et al., 2019; Hawkes et al., 2018; Herzsprung et al., 2016).

Photochemical reactions in natural waters are an important pathway for the modification of DOM; they control the depth of the photic zone and can enhance bioavailability of DOM (Kaiser and Sulzberger, 2004; Gonsior et al., 2014). Photoproduction of fleeting, readily bioavailable nutrients and small oxygenated molecules often support microbial food webs (Wetzel et al., 1995; Zou et al., 2015; Gonsior et al., 2014). The photoproduction of aliphatic molecules from lignins in stagnant peat waters is well documented (Waggoner et al., 2017) and analogously, lightexposure of DOM from the Congo River had produced primarily aliphatic compounds at the expense of aromatic molecules (Stubbins et al., 2010). In the latter study, ~90% of aromatic molecules were lost, and black carbon type and carboxylic-rich alicyclic molecules (CRAM) were found to be more resistant to photo-degradation (Stubbins et al., 2010). Other studies have shown that light exposed highly condensed black carbon photodegraded to less condensed aromatics (Wagner and Jaffé, 2015). While photodegradation of DOM releases small thermodynamically stable endmember CHO molecules (CO2, CO) and water as well as small organic acids (Ward and Cory, 2016), it is also an important pathway for the transformation of heteroatom-containing compounds (e.g. CHNO, CHOP, and CHOS molecular formulas) in natural waters (Ksionzek et al., 2016; Berman and Bronk, 2003). Photoirradiation of heteroatom containing DOM initiated release of ammonia and sulfate (Vähätalo and Zepp, 2005; Ossola et al., 2019), and CHNOS compounds have been reported as highly photo-labile (97% degraded; Stubbins and Dittmar, 2015). However, our knowledge on photodegradation of heteroatom-containing DOM is limited and for example effects to different exposure regimes, including degradation and photoinduced synthesis, remain to be explored.

Photochemical reactions are critical to global nitrogen cycling, where biotic and abiotic conversions between organic CHNO compounds and inorganic nutrients $\mathrm{NH_4^+}$, $\mathrm{NO_2^-}$ and $\mathrm{NO_3^-}$ are well documented (Doane, 2017a, 2017b). The chemical fate of nitrogen and carbon atoms is inextricably connected for organic CHNO compounds. Nitrogen offers an even more rich coordination chemistry than carbon, especially for hydrogen-deficient heterocyclic compounds (Derenne, 2001; Derenne et al., 2012). Alterations of atomic environment, including photo-induced changes, of structural nitrogen in DOM, like tertiary and secondary amines, amides and N-heterocycles, require breaking of chemical bonds with carbon as well. Widespread DOM photo-ammonification (Tarr et al., 2001; Vähätalo and Zepp, 2005; Bushaw et al., 1996), therefore, includes redistribution

of carbon atoms within DOM molecules. Most biological nitrogen occurs in the form of peptides/proteins/amino acids (AAs), N-heterocycles (e.g. nucleic acids and cofactors) and amines. Photo-scission of the amide bond in aliphatic polyamides occurs at 340 nm light to produce amines and aldehydes (Roger et al., 1986), but photodissociation of peptide bonds is retarded in larger biomolecules (Watts and Easton, 2009). Direct photolysis affects the aromatic amino acids Tryptophan and Tyrosine, and to a lesser extent Histidine and Cysteine (Lundeen et al., 2014; Pattison et al., 2012; Tominta et al., 1969) while photoproduced reactive oxygen species ROS, such as hydroxyl radical (•OH: affects all AAs), singlet oxygen (¹O₂: affects His > Trp > Tyr), hydrogen peroxide (H₂O₂: affects Cys and Met), and triplet excited chromophoric organic matter (3CDOM: affect Trp, Tyr, His and Met) cause indirect photochemical damage to AAs, e.g. through radicals and peroxides (Pattison et al., 2012; Lundeen et al., 2014; Remucal and McNeill, 2011). Protein damage initiated by ROS is often responsible for inactivating pathogens, for which reactions of AA side chains are ultimately responsible (Watts and Easton, 2009; Lundeen et al., 2014). These include cross linking of photoactivated aromatic rings (Pattison et al., 2012), formation of peroxides, rearrangements, and ring opening of benzenes, among others. However, the molecular composition of DON is more diverse than merely based on AA derivatives (Yu et al., 2002; Dittmar et al., 2001; McCarthy et al., 2004; Watanabe et al., 2014). While AAs and protein-like DON are generally considered bioavailable (Benner and Kaiser, 2011), significant amounts of bio-recalcitrant DON have also been reported in natural waters (ca. 72%; Vähätalo and Zepp, 2005) including highly aromatic, and even polycondensed DON (dissolved black N) compounds (Wagner et al., 2015a; Ding et al., 2014). Even today, little is known of structural aspects of CHNO molecules in DOM itself and its various organic photoproducts.

Dissolved organic sulfur (DOS) represents the largest pool of sulfur in marine environments, and as such is a critical component of the global S cycle, but the understanding of its sources and transformation mechanisms in freshwaters remains limited (Seidel et al., 2014; Levine, 2016; Levine et al., 2016; Ksionzek et al., 2016; Pohlabeln et al., 2017). A higher complexity of CHOS compounds was reported for deep compared to surface DOM samples in the ocean (Medeiros et al., 2015), likely due to the lack of photo-exposure to the deep-water samples. While abiotic sulfurization of DOM readily operates under anoxic conditions (Seidel et al., 2014, 2017; Pohlabeln et al., 2017), it is likely that under oxidizing conditions photo-oxidation reactions of CHOS molecules might become increasingly important. However, the release of reduced sulfur might contribute to photoproduction of oxygenated CHOS compounds, which were reported to be more photo-reactive than CHO compounds in meromictic lake DOM (Herzsprung et al., 2010). Marine surface DOS was reported to be more photo-reactive compared to the more refractory deep-water DOS (Ksionzek et al., 2016); analogous relationships might operate for CHNO compounds as well. Although photo-production and photo-degradation of DOS and DON have been reported (Herzsprung et al., 2010; Margolin et al., 2018; Mesfioui et al., 2015; Gomez-Saez et al., 2017; Ossola et al., 2019; Gharehveran et al., 2020), the associated reaction mechanisms remain ill-defined.

CHNO and CHOS compounds are commonly more abundant in autochthonous/microbial organic matter sources compared to allochthonous/terrestrial sources (Thorp and Delong, 2002; Sleighter and Hatcher, 2008; Osterholz et al., 2016), and DOM associated with anthropogenic sources was considered rich in heteroatoms N and S (Wagner et al., 2015b; Kamjunke et al., 2019), including heteroatomic dissolved black carbon (DBC; Roebuck et al., 2018). Although protein-like DOM bioavailability has frequently been used as a proxy for DOM lability (Balcarczyk et al., 2009 and references therein), other CHNO compounds have been reported as rather bio-refractory (Vähätalo and Zepp, 2005), depending on the type

and diagenetic history of the DOM under study. In contrast, the bio-lability of DOS was considered as quite low (Seidel et al., 2014; Pohlabeln et al., 2017), and CHOS compounds have been found to be enriched in the refractory, higher molecular weight DOM pool (Seidel et al., 2014; Kang and Mitchel, 2013).

Photo-reactivity of natural DOM mixtures has been shown to be quite complex (Schmitt-Kopplin et al., 1998) and related to its composition, as reflected in optical properties and antioxidant capacity (Mckay et al., 2017). Considering that the understanding of DON and DOS photochemistry remains limited, we hypothesize that both carbon skeleton and heteroatom-containing functional groups will play a role in photochemistry of DOM molecules. Further distinction will arise from the presence of nitrogen-containing molecules because nitrogen can engage in many structural motifs not accessible to either oxygen or sulfur heteroatoms; examples include structural nitrogen such as amide, tertiary amines and various N-heterocyclic molecules which might accumulate following photoirradiation. We have elucidated photo-exposure driven molecular changes of heteroatom containing DOM molecules using a time-sequence photo-exposure encompassing 0, 3, 6 and 13 days in a solar-simulator. The sample used for this study was obtained from a canal collecting freshwater marsh peat soil leachates in the Greater Everglades Ecosystem, draining from a subtropical wetland, with high concentrations of DOC (and associated CDOM), resulting in a DOM sample with low photoexposure history because of efficient CDOM light shielding (Frankovich et al., 2017).

2. Methods

2.1. Sample collection, processing, and laboratory photo-exposure

The Northern Everglades is a mayor DOM supply region to Everglades National Park (Yamashita et al., 2010). The Hillsboro Canal is located in the Northern section of the Everglades and represents a significant drainage system for the peat soils from the Everglades Agricultural Area and characterized by some of the highest DOC levels in this subtropical wetland. The canal system draining the Everglades is hydrologically characterized by slow water velocities and commonly thermally stratified, and as such with minimal physical mixing (McVoy et al., 2011). The sample collected for this study, taken at 4 f. depth, is considered representative of the northern Everglades, peat-derived DOC and likely having undergone only minor photo-exposure (compared to areas further south characterized by lower DOC in more shallow environments). Thus, this sample is ideal for understanding sequential changes in DOM character following photo-exposure for this system. A large ~40 L sample was collected on October 2011. It was subsequently filtered through a 0.7 µM GF/F filter the same day as collection and stored at 4 °C. The sample was concentrated using a 1 kDa regenerated cellulose tangential flow ultrafiltration unit, Pellicon 2 EMD Millipore, until the DOC concentration of the retentate was about 20 times higher than the original sample in order to make it practical to process and analyze the larger samples needed for NMR analysis. During ultrafiltration, the sample was kept chilled in an ice bath and covered in foil to prevent light exposure. The concentrated sample was transferred into seven 500 mL subsamples, four were in quartz flasks and covered with quartz watch glasses while being exposed to simulated sunlight and the other three were in borosilicate glass flasks covered in foil to serve as "dark" controls. Simulated sunlight was produced by a Suntest solar simulator equipped with a xenon lamp (765 W/m² and equivalent to mid-day sunlight on a cloud-free summer day in South Florida) and Solar Standard filter (from manufacturer: simulation of solar radiation outdoors according to DIN 67501:1999), for 0, 3, 6, and 13 days (which is equivalent to about \sim 0, 12, 24 and 52 days of exposure to natural sunlight). Samples were kept at ~30 °C using a recirculating water bath connected to a chilling unit. Following photo-exposure, samples were kept at 4 °C in the dark until size exclusion chromatography (SEC) and optical properties analysis. Samples for NMR and FT-ICR-MS analysis were freeze dried and stored at room temperature until analysis.

2.2. Experimental design

We have used several complementary techniques for determining how photo-exposure alters DOM carbon skeleton and heteroatom-containing functional groups. Measurements of optical properties are relatively quick (\sim 20 min per sample) and require small sample volumes (\sim 10 mL), they detect the absorbing and fluorescing components of DOM, e.g. sp2 hybridized C or aromatic amino acids. Several relationships between optical properties and DOM structure have been developed (e.g., SUVA254 and spectral slopes) as well as DOM source (e.g., the FI for discerning terrestrial versus microbial source) making optical properties a practical method for characterizing DOM. Size exclusion chromatography was chosen to support molecular weight estimates from optical and FT-ICE-MS methods. FT-ICR-MS is a spectroscopic method that determines molecular formulas from DOM compounds that can be ionized, which includes a much broader range of structures than those that can be detected with optical properties. Data collection and processing are more time intensive and the suites of identified formulas usually number in the thousands. With these molecular formulas, DOM compositional metrics can be computed for a wide array of elements, including heteroatoms. ¹H NMR was also used for this study as it gives information about the structure of the DOM molecules including chemical environments of hydrogen and carbon atoms, which is not possible from FT-ICR-MS. The ¹H NMR data provide details about which elements are bound together, which impacts the biogeochemical role that elements may have in the environment. Together this suite of analyses provides complementary of data with coverage that no single method of DOM characterization can provide.

2.3. Dissolved organic matter optical properties

Optical properties were measured within one week of the completion of photo-exposure. Ultraviolet (UV) absorbance was measured on a Varian Cary 50 Bio spectrophotometer from 200 to 800 nm in a 1 cm quartz cuvette. UV–Vis scans were converted to decadic absorbance using a MilliQ water blank and baseline normalized using the average absorbance from 700 to 800 nm. Specific Ultraviolet Absorbance at 254 nm (SUVA $_{254}$, L mg C $^{-1}$ m $^{-1}$) was computed as the decadic absorbance at 254 nm (m $^{-1}$) normalized to DOC concentration (mg C L $^{-1}$) according to Weishaar et al. (2003).

Fluorescence EEMs were measured using a Horiba Jovin Yvon SPEX Fluoromax-3 spectrofluorometer equipped with a 150 W xenon arc lamp, following methods in Yamashita et al. (2010). Briefly, we collected EEMs across excitation wavelengths of 240–455 nm (5 nm increments) and emission wavelengths of 250–695 nm (2 nm increments) using a 1-cm quartz cuvette. Samples were diluted to an absorbance of <0.3 at 254 nm, if needed. Post-processing following Ohno (2002) was applied to EEMs to correct for inner-filter effects and instrument-specific optics. EEMs were normalized based on daily Raman scans to account for potential drift in lamp intensity, and fluorescence intensity was converted to quinine sulfate units following Coble et al. (1993). Daily lamp scans and Raman peaks were used to monitor the monochromator positions, lamp intensity, and spectral shape. A drift of >1 nm from expected peak maximum location indicated that instrument maintenance was needed prior to collecting sample data.

The fluorescence index (FI; McKnight et al., 2001) was computed as the ratio of fluorescence emission intensity at 470 nm to that of 520 nm based on an excitation wavelength of 370 nm (Jaffé et al., 2008). An existing EEM-PARAFAC model ("FCE" dataset on www.openfluor.org) was applied to decompose EEMs into fluorescence components using an alternating least squares algorithm (Bro, 1997). The "FCE" model has been shown to adequately capture the variability in fluorescence characteristics for multiple subtropical wetlands (Hertkorn et al., 2016) and when applied to the samples for this manuscript showed similarly noisy and low intensity residual spectra, indicating a good model fit. Details of the spectral characteristics of the eight model components (C1–C8) established for the FCE model are presented in Chen et al. (2010) and Yamashita et al. (2010), but are briefly described here for general reference. The "FCE" model was

developed with 1394 samples from across the Everglades Agricultural Area and Everglades National Park and produced an eight-component model which was validated according to methods described in Stedmon and Bro (2008). C1 through C6 are humic-like while C7 and C8 are protein-like/phenolic. Within the humic-like group, C4 is consistent with microbial fluorescence characteristics while both C2 and C6 appear to be most prevalent in upstream agricultural regions (Yamashita et al., 2010), with C6 enriched in groundwater relative to surface waters and vice versa for C2 (Chen et al., 2010). For additional details regarding sampling, EEM-PARAFAC modelling and basic spatial and temporal patterns of C1–C8, readers are referred to Chen et al. (2013) and references therein.

2.4. DOM size exclusion chromatography (SEC)

SEC measurements were made within a week of the end of the photoexposure of all samples and were performed on a Thermo Scientific HPLC system equipped with a photodiode array (PDA Plus detector) using a method similar to Maie et al. (2007). Briefly, 1 mL of filtered water was injected onto a BioSep SEC s3000 column. The mobile phase was comprised of 10 mM NaOAc buffer adjusted to pH = 7 with concentrated acetic acid. The UV–Vis detector collected the absorbance at 280 nm. Molecular weight and polydispersity were computed according to Maie et al. (2007) from the sample chromatograms and those of polystyrene standards.

2.5. Ultrahigh-resolution FT-ICR-MS analysis

Ultrahigh-resolution Fourier transform ion cyclotron mass spectra were acquired using a 12 T Bruker Solarix mass spectrometer (Bruker Daltonics, Bremen, Germany) hyphenated with an electrospray ionization source in negative mode. Samples were diluted with MeOH and then injected into the electrospray source using a micro-liter pump at a flow rate of 120 μLh⁻¹ with a nebulizer gas pressure of 138 kPa and a drying gas pressure of 103 kPa. A source heater temperature of 200 °C was maintained to ensure rapid desolvatation in the ionized droplets. Spectra were systematically calibrated using NOM reference list. The spectra were acquired with a time domain of 4 megawords from m/z 147.4 to 1000. Data processing was done using Compass Data Analysis 4.1 (Bruker, Bremen, Germany) and formula assignment was made by in-house made software (NetCalc) using a restricted list of small molecular units with defined mass differences using NetCalc software (Tziotis et al., 2011) to define compositional relationships from networks for CHO, CHNO and CHOS molecular series. A hierarchical clustering approach was performed on the normalized data (Hierarchical Clustering Explorer 3.5, Maryland, USA) using average linkage and Pearson correlation coefficient as similarity search allowing to discriminate samples without prior knowledge of data classification.

2.6. Nuclear magnetic resonance spectroscopy (NMR)

Dried DOM samples in glass flask were first exposed to D_2O to obtain the water-soluble fraction of DOM, and the remainder (\sim 5% based on 1H NMR integral) was dissolved in CD_3OD . Presence of lipid-like molecules in the methanol fraction validated our initial concern that not all organic molecules of DOM would redissolve in water after drying because of the potential effects of hydrophobic collapse (Chin et al., 1998). Complete drying was necessary because of exchange of protonated solvents by deuterated counterparts for NMR spectroscopy.

 1H NMR spectra of DOM extracts were acquired with a Bruker Avance III NMR spectrometer at 800.13 MHz (B $_0=18.7$ T) at 283 K from a very few mg (D $_2$ O) and $\sim \! 50~\mu g$ of solid (CD $_3$ OD) obtained by evaporation of original methanol-h $_4$ solution, dissolved in approx. 130 μL CD $_3$ OD (Merck. 99.95% 2H) solution with a 5 mm z-gradient $^1H/^{13}C/^{15}N/^{31}P$ QCI cryogenic probe (90° excitation pulse: $^1H\sim 10~\mu s$) in sealed 2.5 mm Bruker MATCH tubes. 1-D 1H NMR spectra were recorded with a spin-echo sequence (10 μs delay) to allow for high-Q probe ringdown, and classical pre-saturation to attenuate residual water present "noesypr1d", typically 512–2048 scans (5 s acquisition time, 5 s relaxation delay, 1 ms

mixing time; 1 Hz exponential line broadening). Area-normalized 1H NMR spectra (total 1H NMR integral =100%) were computed from full-resolution 1H NMR spectra (δ_H : 0.5–8.2 ppm) with exclusion of methanol and water.

3. Results and discussion

3.1. Photoirradiation induced changes in optical properties and molecular weight

CDOM was bleached by photo-exposure as seen in the decreasing A_{254} with increasing time of exposure (overall reduction by 50%; Table 1). Similarly, total fluorescence declined drastically from ca. 7200 to 251 (reduction by 96%; Table 1), suggesting the preferential degradation of certain aromatic molecules. On the other hand, fluorescence index (FI) did not change between t=0 and t=6, marginally from t=6 to t=9, but considerably from t=9 to t=13 (Table 1). This suggests that the FI was less sensitive to molecular changes taking place for the first nine days of irradiation but started changing more significantly with further bleaching.

Some of the PARAFAC components showed higher sensitivity to molecular changes during the first nine days of irradiation. C6, a microbial humic-like component that has been shown to be photo-labile in other Everglades samples (Chen et al., 2010) was completely absent in any of the photo-exposed samples, while the unexposed t=0 and dark control samples had similar relative abundances of C6. In contrast, C3 showed a significant increase in its abundance followed by a slower decrease with further light exposure and the photo refractory C2 component consistently increased in relative abundance. This is in agreement with the proposed role of C3 as an intermediate in the photo-degradation of C6 to C2 as previously suggested (Chen et al., 2010). Similar to C2, C4 increased steadily with light exposure, but at a much lower rate compared to C2. C1, the humic-like, and

 $\label{thm:computed} \textbf{Table 1} \\ \textbf{Computed mass ions of singly charged negative ESI ions of DOM samples before and after photo-irradiation including optical indices (i.e., FI: fluorescence index, Abs^{254-nm}: absorbance at 250 nm, TF: Total fluorescence and Sr: optical proxy for molecular weight) and molecular weight distribution. \\ \end{table}$

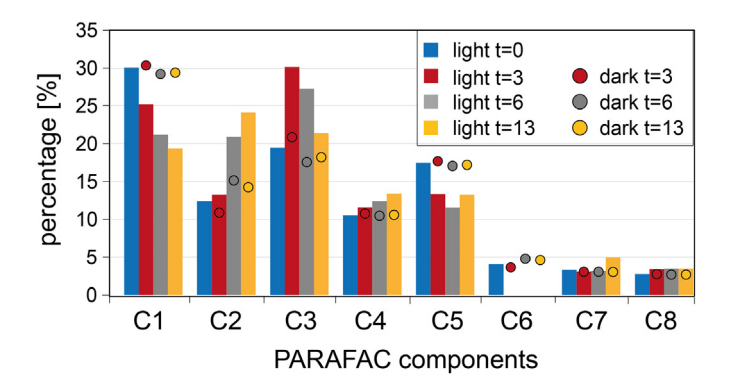
| | t ₀ (initial) | $t_{3 \text{ Days}} (h\nu)$ | t _{6 Days} (h ν) | t _{13 Days} (hν) |
|-------------------------------------|--------------------------|-----------------------------|--------------------------------|---------------------------|
| Optical properties | | | | |
| FI | 1.30 | 1.30 | 1.29 | 1.22 |
| Abs ^{254nm} | 7.59 | 6.35 | 4.98 | 3.12 |
| TF | 7199 | 1304 | 770 | 251 |
| Sr | 0.98 | 0.93 | 1.06 | 1.09 |
| Molecular weight distribution | | | | |
| Mw (weight avg. MW) | 1321 | 1031 | 820 | 754 |
| Mn (number avg. MW) | 418 | 306 | 247 | 232 |
| d (polydispersity) | 3.16 | 3.37 | 3.31 | 3.25 |
| Members of molecular series | | | | |
| Intensity mass weighted average m/z | 386 | 386 | 377 | 369 |
| CHO | 1557 | 1697 | 1622 | 1415 |
| | (54.8%) | (51.5%) | (50.4%) | (46.6%) |
| CHOS | 299 | 336 | 364 | 295 (9.7%) |
| | (10.5%) | (10.2%) | (11.3%) | |
| CHNO | 983 | 1260 | 1233 | 1329 |
| | (34.6%) | (38.3%) | (38.3%) | (43.7%) |
| Total number of assigned mass peaks | 2839 | 3293 | 3219 | 3039 |
| Intensity average H [%] | 48.06 | 47.78 | 48.03 | 47.89 |
| Intensity average C [%] | 37.87 | 37.52 | 36.96 | 36.41 |
| Intensity average O [%] | 13.50 | 14.07 | 14.33 | 14.88 |
| Intensity average N [%] | 0.46 | 0.54 | 0.55 | 0.70 |
| Intensity average S [%] | 0.10 | 0.10 | 0.13 | 0.12 |
| Intensity average H/C ratio | 1.27 | 1.27 | 1.30 | 1.32 |
| Intensity average O/C ratio | 0.36 | 0.38 | 0.39 | 0.41 |
| Intensity average C/N ratio | 81.6 | 69. 6 | 66.7 | 52.2 |
| Intensity average C/S ratio | 391.9 | 377.4 | 291.7 | 292.7 |
| Intensity average DBE | 7.95 | 7.95 | 7.30 | 6.92 |
| Intensity average DBE/C | 0.210 | 0.212 | 0.197 | 0.190 |

commonly most abundant PARAFAC component in the Hillsboro Canal sample decreased steadily with increasing photo-exposure, while humic-like C5 decreased mainly until t=3 but not much thereafter. Unlike the other six PARAFAC components, the protein-like components C7 and C8 did not change much in relative abundance with prolonged light exposure, except for a slight increase for C7 after 13 days (Fig. 1). The trends in PARAFAC components suggest some photo-stability of certain protein-like components and susceptibility of the more aromatic, humic-like components (C1 and C6) to photodegradation, and the enrichment in the most photo-refractory components (e.g. C2 and C4 and to some degree C3).

Estimates of molecular weight (MW) changes by the three methods used showed slightly different trends although all three produced an overall decrease between the unexposed and longest exposure sample. Values for the optical proxy for molecular weight (Sr) suggested an increase in MW after 3 days followed by a decrease with further light exposure. This apparent decoupling of Sr (and MW) with photo-exposure time suggests a complex photo-processing mechanism, possibly indicating an initial photohumification process, followed by photodecomposition into lower mass molecules. The MS-derived weighted average mass-to-charge (m/z) ratios did not show an increase or decrease between the unexposed and shortest exposure time (t = 3) but did show a decrease in MW for the longer exposure times (Table 2). The SEC-derived MW distribution profile of DOM showed a consistent evolution toward lower MW with increased photoexposure for all samples with the largest size molecules (shortest retention time) affected most (Table 1, Fig. S1). Photoproduction (higher SEC absorbance signal) primarily affected the lower MW region of the SEC chromatogram, suggesting not only the preferential degradation of higher MW compounds, but a production of lower MW compounds as well (see also below).

3.2. Photoirradiation induced changes in DOM structural characteristics using $^1\mathrm{H}$ NMR spectroscopy

Standard solution-state 1H NMR spectra of DOM show chemical environments of non-exchangeable protons bound to various types of carbon atoms and are particularly well suited to depict relative abundance and speciation of aliphatic groups, which leave less conspicuous signatures in fluorescence and mass spectra (Gonsior et al., 2018). Dried DOM samples were first exposed to D_2O to obtain the water-soluble fraction of DOM; then, CD_3OD was added to get access to potential water insoluble DOM fractions conceivably produced in the process of drying. Not all DOM was found soluble in D_2O because we could observe $\sim 5\%$ of DOM (by 1H NMR integrals) with aliphatic and lipid-like molecules in the methanol fraction (Figs. 2, S6, S8). The presence of these molecules in appreciable amounts validated our long-standing concern that not all organic molecules of DOM would redissolve in water after drying because of the potential effects of hydrophobic collapse. Here, extended aliphatic systems agglomerate by virtue of non-polar and noncovalent van der Waals interactions, and these aggregates cannot be entirely



disrupted by water alone (Chin et al., 1998). Complete drying prior to exchange of protonated by deuterated solvents used in NMR spectroscopy is an indispensable sample preparation in case of mass limited samples that are also complex mixtures of (many thousands of) organic molecules. 1H NMR spectra of the water-soluble fraction of DOM (in D_2O) and of the comparatively minor (~5% according to NMR integrals) water insoluble fraction (in CD_3OD) showed congruent evolution of fundamental specific proton and carbon chemical environments during photo-irradiation (Figs. 2, S2–S9; Tables 2, S1 and S2). Water soluble DOM featured considerably higher proportions of carboxylic acids (25% vs. 15% $C\alpha H$ units), functionalized (38% vs. 28% OCCH units) and oxygenated aliphatics (24% vs. 16% OCH units), while alkyl derivatives were more abundant in the methanol solution (50% vs. 33%) (cf. Figs. 2, S2–S9, Tables 2, S1, S2).

The temporal evolution of fundamental (Figs. S4, S7; Table 2) and more detailed (Figs. S6, S9; Tables S1, S2, S3, S6, S8) DOM substructures was more uniform for the methanol than for the aqueous fraction. This reflected most likely a smaller overall molecular diversity of methanolic compared with aqueous DOM and lower proportions of oxygenated functional groups. A depletion of remotely oxygenated aliphatic groups in methanolic DOM caused most of alkyl protons to resonate in a rather narrow bandwidth $(\delta_{\rm H} \sim 1.27 - 1.32 \text{ ppm})$; in contrast, alkyl protons in aqueous DOM resonated from $\delta_{\rm H} \sim 0.9$ –1.7 ppm (Figs. 2, S2, S3), indicative of a more complex remote alkylation and oxygenation in aqueous than in methanolic DOM. The ¹H NMR spectra of the initial non-irradiated aqueous and methanolic DOM (t = 0) were distinct from those of the irradiated samples (t = 3, 6, 13) demonstrating active photo-transformations for both DOM from the onset of irradiation (Fig. S6), but hierarchical cluster analysis (Fig. 2B) also demonstrated closer resemblance of t = 0, t = 3 versus t = 6, t =13 samples, suggesting a complex non-linear photo-evolution of DOM substructures that was mainly driven by overall congruence of carboxylic acids, aliphatic (poly)oxygenation, olefin photoproduction and decomposition of oxygenated aromatics (cf. below).

The ¹H NMR spectrum of the non-irradiated aqueous DOM sample showed distinctly higher proportions of a broad ¹H NMR resonance indicative of aliphatic groups (CCCH units; $\delta_{H} \sim 0.8\text{--}2.0$ ppm) and of all aromatic compounds ($C_{ar}H$; $\delta_H \sim 6.5$ –8.2 ppm) and lower proportions of oxygenated aliphatics (OCH units; $\delta_H \sim 3.1$ –5.2 ppm) and olefins (= CH; $\delta_H \sim 5.5$ –6.0 ppm) compared with all other samples (Figs. 2, S6). The most obvious feature was the continual decline in abundance of phenolic (and C_{ar}O units) at $\delta_{H} \sim$ 6.5–7 ppm during photo-irradiation (Figs. 2, S6), whereas common aromatic molecules with aliphatic substituents ($\delta_H \sim 7$ -7.3 ppm) and polycarboxylated aromatics, and possibly six membered nitrogencontaining heteroyclic molecules, and polycyclic aromatic compounds (δ_H \sim 7.3–8.2 ppm) even increased temporarily in relative abundance (at t = 6; Figs. 2, S4, S6) to eventually decline as well. The section from δ_H 7.4-7.8 ppm which comprised singly carboxylated benzenes, grew initially from t = 0 through t = 3 and then progressively declined, in particular between $\delta_H \sim 7.6\text{--}7.8$ ppm. Deshielded protons at $\delta_H > 8.2$ ppm returned to initial relative abundance following an initial increase (Figs. S2, S5, S6), suggesting polycarboxylation of benzenes rather than six membered ring N-heterocycles or polycyclic aromatic compounds, which are considered rather photolabile (Fasnacht and Blough, 2002). Substituted olefins (δ_H ~ 5.3-6 ppm) continually increased in relative abundance, suggesting not only the preferential photo-degradation of aromatic compounds in comparison with olefins, but also photoproduction of olefins, possibly by elimination of water from aliphatic alcohols (Hjerrilg et al., 2020). Hence, olefins at t = 0 likely represented processed natural products whereas olefins at t > 0primarily represented photoproducts.

Comparison of unsaturated $C_{\rm sp2}H$ protons in 1H NMR spectra and PARAFAC components showed concordant temporal evolution of abundance for component C3 and (poly)carboxylated aromatic acids, with a relative maximum at t=3. It is agreed upon that fluorescence-active chromophors depend on the presence of $C_{\rm sp2}$ -based (aliphatic and aromatic) unsaturation, which also produced 1H NMR resonances at $\delta_H > 5$ ppm. 1H NMR spectra demonstrated continual increase in abundance during irradiation, as did PARAFAC components C2, C4, and C7, with C2

Table 2 ¹H NMR section integrals (800 MHz, D2O and CD3OD) of re-dissolved freeze-dried DOM at different times of photoirradiation, resolved into gross substructures.

| δ(¹ H) [ppm] Key substructure | Key substructures | $\frac{D2O}{t=0}$ | $\frac{D2O}{t=3}$ | $\frac{D2O}{t=6}$ | $\frac{D2O}{t = 13}$ | $\frac{\text{CD3OD}}{\text{t} = 0}$ | $\frac{\text{CD3OD}}{\text{t} = 3}$ | $\frac{\text{CD3OD}}{\text{t} = 6}$ | $\frac{\text{CD3OD}}{\text{t} = 13}$ |
|---|-------------------|-------------------|-------------------|-------------------|----------------------|-------------------------------------|-------------------------------------|-------------------------------------|--------------------------------------|
| | | | | | | | | | |
| 7.0–8.2 ppm | CarH | 3.2 | 3.6 | 2.5 | 2.1 | 2.2 | 2.0 | 1.9 | 1.6 |
| 5.2-7.0 ppm | = CH, O2CH | 0.9 | 1.3 | 2.0 | 1.6 | 1.1 | 0.9 | 1.6 | 2.3 |
| 3.1-4.7 ppm | OCH | 22.8 | 25.3 | 24.6 | 23.7 | 10.8 | 16.8 | 16.4 | 16.6 |
| 1.8-3.1 ppm | OCCH | 38.7 | 38.5 | 40.1 | 40.1 | 29.8 | 31.7 | 27.6 | 28.0 |
| 0.5-1.8 ppm | CCCH | 34.5 | 31.3 | 30.7 | 32.4 | 56.0 | 48.6 | 52.6 | 51.4 |

showing the most congruence in relative abundance to respective $^1\mathrm{H}$ NMR resonances. With the available limited data from four samples, we cannot assess the relevance of these superficial correlations at present.

Interestingly, the relative proportions and the bandwidth of ^{1}H NMR resonances of purely aliphatic units considerably declined (CCC<u>H</u> units; $\delta_{H} \sim 0.5$ –1.25 ppm), and remotely oxygenated branched functionalized

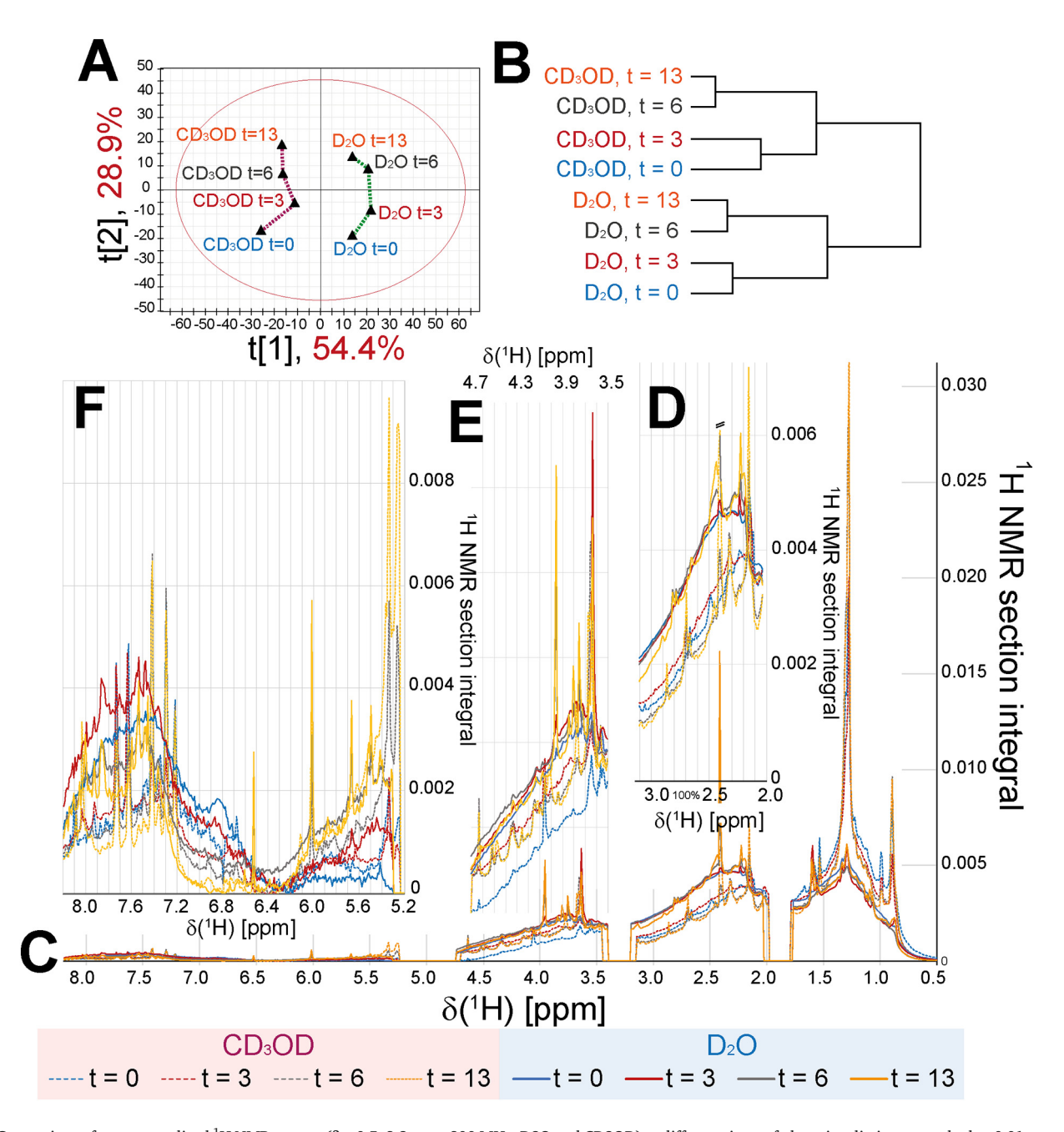


Fig. 2. Comparison of area-normalized 1H NMR spectra (δ_H : 0.5–8.2 ppm; 800 MHz, D2O and CD3OD) at different times of photo-irradiation, smoothed to 0.01 ppm (8 Hz) for improved discrimination of spectral features in overlay. Panel A: hierarchical cluster analysis HCA and (panel B) principal component analysis (PCA). Panel C: entire spectrum, with exclusions of CD3OD and D2O section of $C_{sp2}H$ units. Panel D: section of functionalized OCC $\underline{\underline{H}}$ units, Panel E: section of oxygenated aliphatic OCC $\underline{\underline{H}}$ units, Panel F: section of $C_{sp2}\underline{\underline{H}}$ units.

aliphatic units (OCCH units; $\delta_H \sim 1.35$ –1.95 ppm) also considerably decreased during the initial three days of photo-degradation. As a result, an increasing relative abundance of likely photo-produced oxygenated aliphatic units (OC_{al}H-units; $\delta_H \sim 3.1$ –5.24 ppm) and aliphatic carboxylic acids (HOOC-C αH -units; $\delta_H \sim 2.1$ –2.5 ppm) was observed. The apparent initial decrease of aliphatic-rich lipid-like compounds (CCCH-units; $\delta_H \sim$ 0.7–2.0 ppm) was more difficult to justify because these primarily $C_{sp3}H$ units should be rather photo-inert. Here, the overall shape of the ¹H NMR resonance becomes relevant, as the near featureless broad humplike ¹H NMR resonance signal at t = 0 got sharper at t = 3, implying an overall decrease in the diversity of aliphatic branching, in particular for extended branched open and alicyclic alkyl groups. These components carry higher proportions of secondary and tertiary carbon atoms that more efficiently stabilize radicals than smaller open chain alkyls, which might initiate photooxidation of CH units by e.g. hydroxyl radicals (Glrigorovski et al., 2015). Photoproduction caused a progressive increase in relative abundance of sharp ${}^{1}H$ NMR resonances (from t = 3 through t = 13 across the entire spectrum); these represented a diversity of small, oxygenated molecules (Schmitt-Kopplin et al., 1998), each contributing to less than one thousandth of total NMR integral.

 ^1H NMR spectra are well suited to differentiate OCH, OCCH and CCH based chemical environments because remote effects of oxygen on ^1H NMR chemical shifts (δ_H) are stronger and better defined than those of N and S; in fact, the δ_H of NCH and SCH units overlap with those of remotely oxygenated OCCH units. Without employing direct detection (very insensitive) ^{15}N NMR spectroscopy, unambiguous determination of CHNO chemical environments from ^1H NMR spectra alone will remain ambiguous and has not been attempted. However, high-resolution mass spectrometry is very well suited to analyze CHNO and CHOS compounds (cf. below).

3.3. Photoirradiation induced changes in DOM molecular composition using FT-ICR-MS

Ultrahigh-resolution Fourier transform ion cyclotron mass spectra (FT-ICR-MS) of DOM samples before and upon irradiation provided several thousand mass peaks for any single sample, of which many hundreds were assigned to extended CHO, CHNO and CHOS molecular series (Valle et al., 2020; Niu et al., 2019; Hertkorn et al., 2016). Nearly all of the assigned molecular compositions changed in relative abundance with progressive light exposure (Fig. 3; Tables 1, S3). Both van Krevelen and O/C versus mass-to-charge (m/z) diagrams showed significant molecular changes in aliphatic, oxygen-rich and highly unsaturated regions (Fig. 3, Table S3). Photoproduction of highly oxygenated compounds (i.e., 0.66 < O/C < 1and 0.93 < H/C < 2.23) suggests a wide range of polyol-like entities (Niu et al., 2019) was accompanied by the depletion of oxygen-deficient molecules with a O/C ratio between 0.03 and 0.2 (Fig. 3B). Successive losses of highly unsaturated compounds occurred, particularly for the two earliest irradiation times (Fig. 3A), and all of those showed H/C and O/C ratios representative of condensed aromatic compounds (i.e., 0.5 < H/C < 1.0 and 0 < O/C < 0.16). The presence of oxygenated compounds, potentially lipid-like aliphatic molecules, after photo-processing agreed with previous findings in which ligninlike and/or condensed tannin-like compounds produced high proportions of oxygen-rich aliphatic compounds following exposure to singlet oxygen (102) and hydroxyl radicals (•OH) (Waggoner et al., 2017; Niu and Croué, 2019; Gonsior et al., 2014, 2017). These are, together with triplet excited state ³CDOM, the key reactive oxygen species (ROS) (Mckay et al., 2017), which act as photosensitizers for processing of DOM (Zepp et al., 1977; Mopper and Zhou, 1990; Niu and Croué, 2019; Niu et al., 2019). This behavior is consistent with the hypothesis that aromatic substances and unsaturated

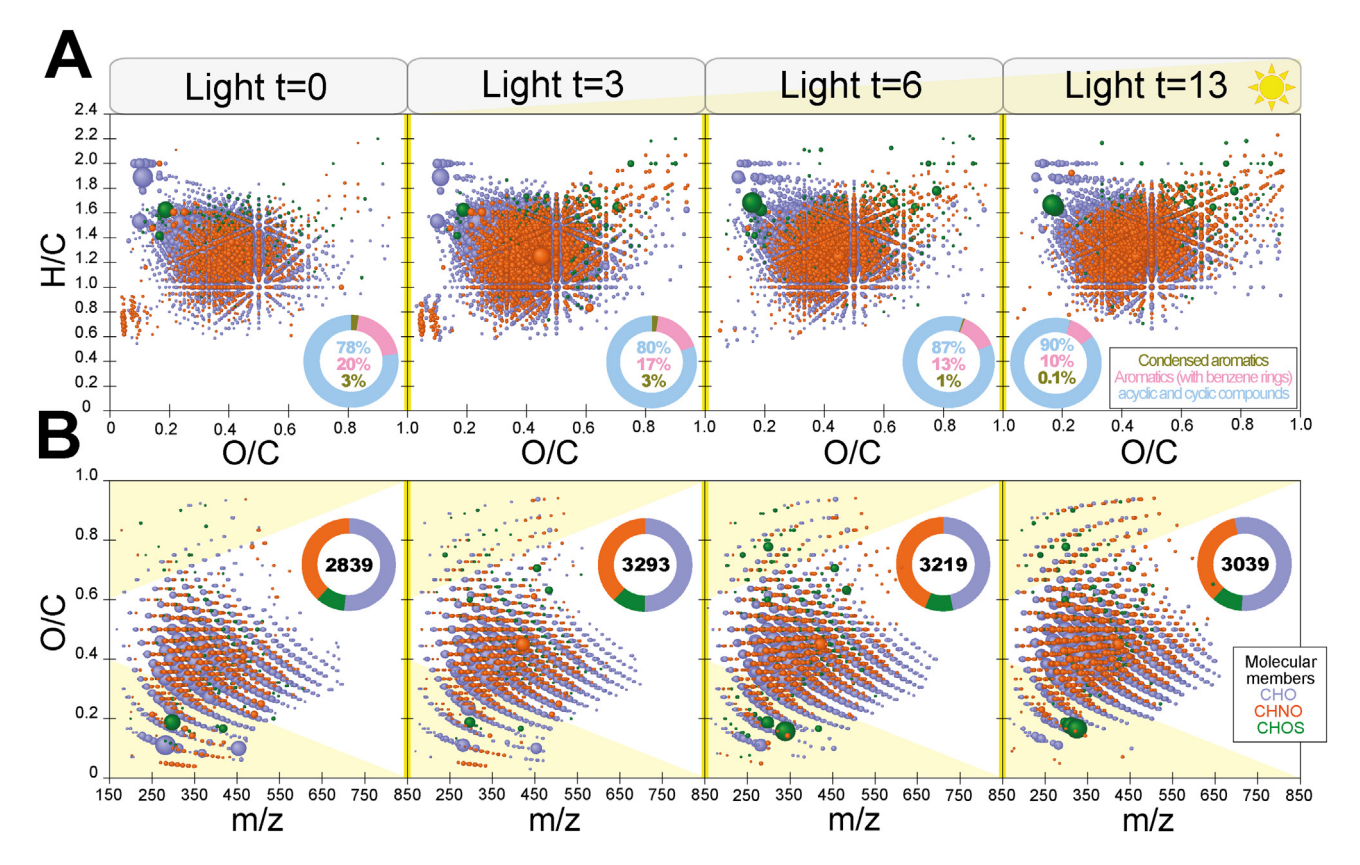


Fig. 3. Visualizations of negative electrospray 12 T FTICR mass spectra of DOM sample before and during irradiation experiments, with color code for molecular series as follows: blue (CHO), green (CHOS) and orange (CHNO). Bubble areas reflect the relative intensities of each mass peak. Panel A: H/C versus O/C van Krevelen diagrams. Ring histograms depict the computed percentage of condensed aromatics, aromatics (benzene rings) as well as alicyclic and acyclic compounds using aromaticity equivalent (AI) (Yassine et al., 2014). Panel B: mass-edited H/C ratios; yellow triangle is provided for better distinction of photoproduced highly oxygenated molecules. Ring histograms represent the relative proportions of the assigned CHO, CHOS and CHNO molecular compositions, with total number of assigned negative ions (see Tables 1, S3).

compounds are preferentially photodegraded, moving the average H/C toward higher values (Tremblay et al., 2007; Gonsior et al., 2009). These processes most likely refer to self-sensitized photooxidation and/or photochemical alterations of DOM materials upon irradiation, originating from cleavage of covalent bonds or non-specific molecular interactions between CDOM and other chemical constituents (Niu et al., 2016; Sharpless et al., 2014).

In addition, we observed an initial increase of the total number of CHO molecular formulas from 1557 to 1697 between t=0 and t=3, followed by a decrease to 1622 and 1415 at t=6 and t=13, respectively. A shift toward higher numbers of oxygen atoms within CHO molecules was particularly pronounced from t=0 to t=3 (Fig. 5). A decrease in Sr suggesting a slight increase in MW, possibly due to the removal of small and photoreactive compounds and/or possible photo-humification reactions was also observed. Like the trend in Sr, where little change was observed between the un-exposed sample and shortest photo-exposure sample, the intensity mass weighted average m/z was highest at t=0 and t=3 but decreased thereafter with further light exposure. Polydispersity according to SEC data decreased with increasing exposure time, which is mostly consistent with the trend in decreasing number of molecular formulas detected with FT-ICR-MS with increasing photo-exposure time.

FTMS-based hierarchical cluster analysis (HCA) clearly differentiated two main groups, classified based on duration of light exposure, revealing a strong similarity between the two short photo-exposure samples (t = 0and t = 3) on one hand, and longer time photoirradiation experiments (t = 6 and t = 13, Fig. 4A) on the other hand. In general, the molecular variances were more prominent at low molecular weight after 6 and 13 days of light-exposure (Fig. 4B-D), in agreement with SEC results. Indeed, Fig. 4C shows a significant number of molecular components consistent with a mixture of highly unsaturated compounds and carboxylic-rich alicyclic molecules (CRAM, Hertkorn et al., 2006) at t=0 and t=3. Consistent with the susceptibility of unsaturated molecules to photo-degradation, the DBE decreased by one unit value (from 8 to 7), and the H/C ratio increased steadily from 1.27 to 1.32 between t = 0 and t = 13 (Table 1). Similarly, the O/C ratio increased from 0.36 to 0.41, suggesting that the bulk DOM changed to a more aliphatic, less unsaturated, and more oxidized composition with increased photo-exposure (Table 1).

3.4. Photoirradiation induced variances in unsaturation and oxygenation levels

Molecular compositions associated with DBE-O values were computed for each experiment before and after irradiation, and the photoinduced effects on the unsaturation level in the DOM mixture is shown in Fig. S11. The total number of molecular formulas at lower DBE-O value increased upon irradiation, which is reflected by the increased number of compounds with the same DBE-O values. These variations in DBE-O values with light exposure support the hypothesis that unsaturated compounds are highly photoreactive, in agreement with similar trends observed for Mangrove, Riverine and Estuarine DOM (Tremblay et al., 2007; Rodriguez-Zuniga et al., 2008; Gonsior et al., 2009). Indeed, DBE-O values were evenly distributed in the ranges (-14 to 10) and (11 to 20) in all experiments. While the samples at t=0and t = 3 appeared to contain highly unsaturated compounds with DBE and DBE/C values of 8 and 0.21 (Table 1), respectively, likely due to their lack of historically significant exposure to light, a progressive loss of compounds with DBE-O values between 11 and 20 at longer light exposure times (t = 13) was clearly observed. Overall, there was an apparent displacement from higher to lower DBE-O values upon irradiation, particularly for samples at t = 6 and t = 13, in agreement with previous studies where the preferential photodegradation of unsaturated compounds was reported (Kujawinski et al., 2004; Gonsior et al., 2009; Stubbins et al., 2010).

The molecular compositions that were unique either in sample t=0 prior to irradiation or in each experiment following irradiation (t=3,6,13) are shown in Fig. 6A–B. Clearly, entire classes of molecular compositions with different levels of unsaturation were photo-degraded while others were generated (Fig. 6C–D). This illustrates and confirms our discussions above regarding the photo-transformation of unsaturated and

aromatic compounds (high DBE-O) to more saturated compounds (low DBE-O). In fact, this shift from high to low DBE-O values (increase of molecules rich in oxygen atoms at the expense of those rich in carbon-carbon double bonds), was probably due to an increase in proportions of oxygen-containing functional groups such as carboxyl (-CO₂H) and hydroxyl (C-OH), and photooxidation of olefins during light exposure (Kujawinski et al., 2004; Gonsior et al., 2009; Vähätalo, 2009; Stubbins et al., 2010). While 1954 molecular formulas were produced upon irradiation, only 324 were lost upon irradiation (Fig. 6C). Elemental analysis showed photo-production of 666 CHO compounds, 976 CHNO compounds, and 312 CHOS compounds. A relative decrease in the number of CHO

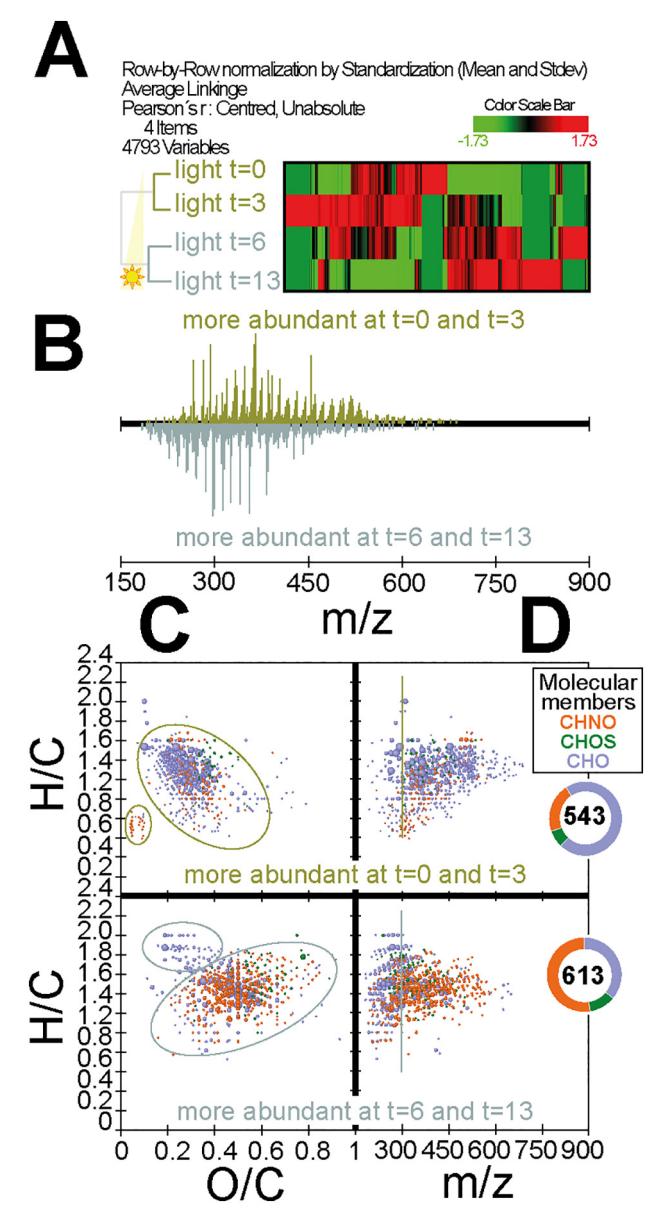


Fig. 4. Comparative analysis of negative electrospray 12 T FT-ICR mass spectra of DOM samples before and upon photoirradiation experiments (light exposure t = 3, 6 and 13 days). (panel A) Clustering analysis based on the similarity values between the spectra of four experiments using average linkage and Pearson correlation on normalized FT-ICRMS data. Heatmap is visualizing the masses responsible for the clustering. (panel B) Visualization of the abundant mass peaks at t = 0, 3 days (olive color) compared to t = 6, 13 days (blue gray color), respectively. (panel C) van Krevelen plots. (panel D) mass edited H/C ratios. Bubble reflect the averaged abundance of respective mass ion. Ring histograms represent the relative proportions of the abundant CHO, CHOS and CHNO molecular compositions.

compounds, associated with an increase in CHNO compounds upon irradiation, has been reported previously (Sleighter and Hatcher, 2008). On the other hand, molecular compositions representative of photo-consumed compounds were in the order CHO (145 formulas), CHNO (111 formulas) and CHOS (68 formulas). These relationships between photo-consumed and photo-produced molecular compositions suggest a strong effect of

heteroatom-containing functional groups on DOM-related photochemistry and a relatively higher photo-recalcitrance of CHNO compounds. As such, light exposure not only modifies the molecular compositions of DOM but plays an essential role in the photodegradation and photoproduction of hetero-atom DOM, which may be more bioavailable than the original structures when released into the environment.

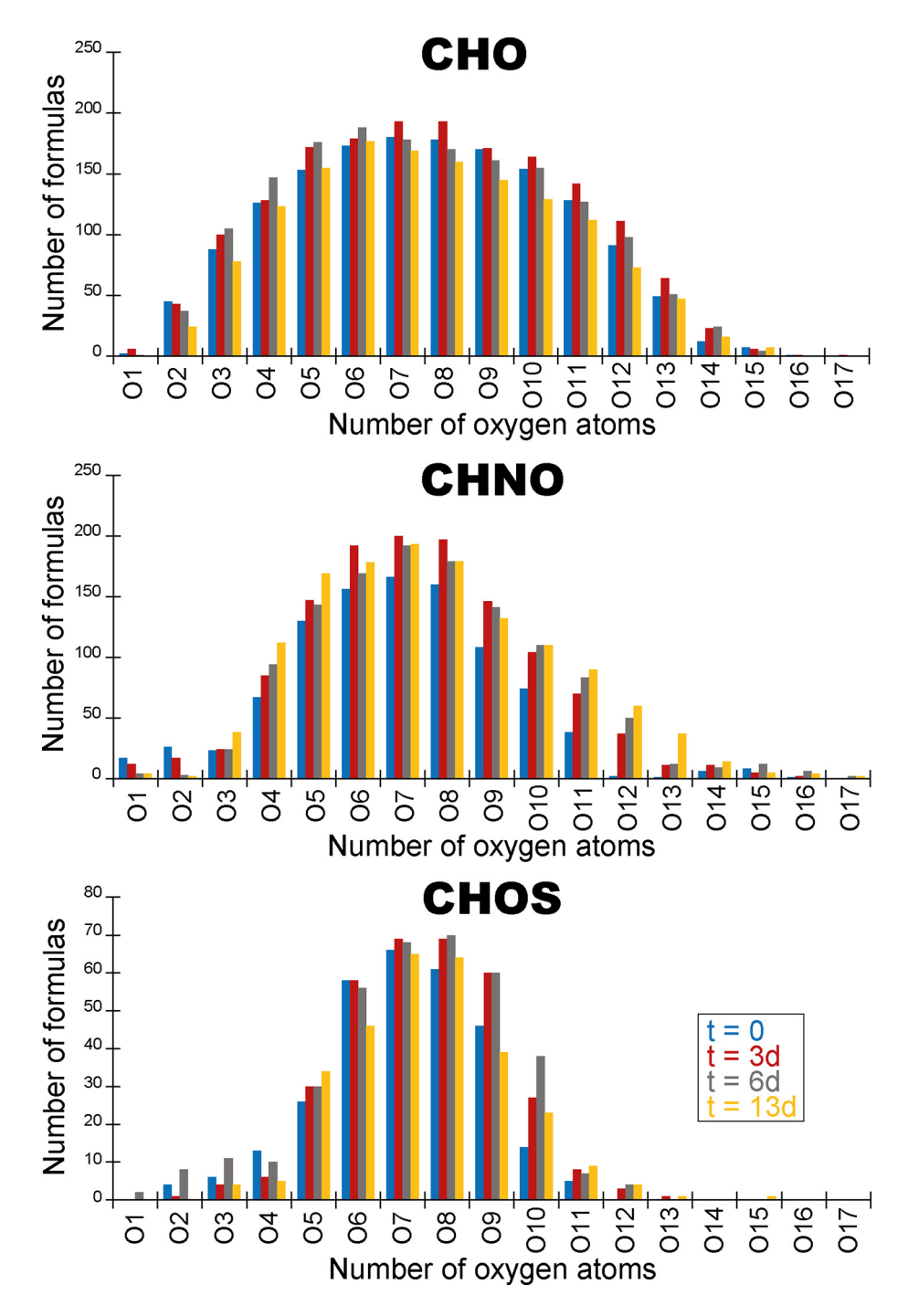


Fig. 5. Counts of assigned molecular formulas sorted according to specific numbers of oxygen atoms demonstrate different photo-evolution from t=0 through t=13 for the molecular series CHO, CHNO and CHOS. Distinction between the non-irradiated sample (t=0) and all others was maximal for oxygen-rich CHNO and, less extensive, for oxygen-rich CHOS molecules while CHO compounds showed highest counts at t=3 except for highly oxygen-depleted molecules (cf. text). The distribution of CHNO and CHOS compounds is narrower than that of CHO compounds. While some structural nitrogen occurs independent from oxygen it might not dominate here because the low count oxygen CHNO compounds ($O \le 4$) are depleted. This also applies to CHOS compounds ($O \le 5$) but probably results from the presence of oxygenated functional groups $-S_nO_mH$. The depletion of high oxygen count CHOS compounds ($O \ge 10$) compared with CHO compounds is remarkable because it denotes a fundamental distinction of the CHO-part within CHO and CHOS compounds. This might be intrinsic but modulated by ESI[-] based ionization selectivity, which however favors observation of sulfonic acid derivatives (Gonsior et al., 2011).

3.5. Photoirradiation induced changes in the heteroatom composition of DOM

While the total number of molecular formulas of CHO slightly decreased between t = 0 and t = 13 (from 1557 to 1415), the total number of assigned mass peaks increased significantly from 2839 to 3039 (Table 1). This increase resulted from the significant number of newly assigned, photo produced CHNO compounds, which changed from 983 (t = 0) to 1329 (t = 13), leading to a decrease of the C/N ratio from about 82 to 52. In contrast, the total number of CHOS molecules remained near constant between t=0 and t=13 (299 to 295), but the C/S ratio decreased from 392 to 293, indicating a relative enrichment in CHOS compounds with increased light-exposure (Table 1). A short-term relative increase from t = 0 to t = 6 was observed for CHOS compounds (from 299 to 364), while the increase of CHNO compounds was continuous from t = 0through t = 13 (Table 1). This suggests that some of the dynamics of CHOS compounds might be linked to PARAFAC component C3, a proposed intermediate in the transition from C6 to C2 (Chen et al., 2010, 2013), while the CHNO components seem to reflect a high degree of photostability and as such might be linked to the enrichment of C2 during light exposure time. While novel CHNO and CHSO components generated at intermediate irradiation times (t = 3 and 6) might be linked to C3, those associated with the final exposure time of t = 13 might be more liked to C2, while those present at t = 0 and completely removed at t = 3 are might be linked to C6 (see Fig. 4).

MS-derived hierarchical cluster analysis showed similarity of $t=0,\,t=3$ and $t=6,\,t=13$ samples (Fig. 4A) as observed in 1H NMR spectra (cf. above), in which primarily CHO compounds of intermediate unsaturation (H/C $\sim 1.2\pm0.4$) and oxygenation (O/C $\sim 0.25\pm0.1$) dominated. In comparison, late stage photo-irradiated samples showed higher proportions of less unsaturated CHNO compounds (H/C $\sim 1.4\pm0.2$) with a rather high oxygenation (O/C $\sim 0.5\pm0.15$), while late stage CHO compounds were of low mass (m/z<400) but formed two classes in van Krevelen diagrams: a deoxygenated rather saturated group (H/C $\sim 1.4\pm0.2$ and O/C $\sim 0.45\pm0.15$) and a nearly saturated one (H/C $\sim 1.8\pm0.2$ and O/C $\sim 0.25\pm0.15$).

Overall, both photoproduction and photodecomposition of CHO, CHOS and CHNO compounds likely occurred during the light exposure time series (Figs. 4–6, S12; Table S3). For example, Table S4 shows comparisons between shared and unique molecular formulas for each time series compared

to t=0. For the CHNO compounds, shared formulas for each time series with t=0 decreased somewhat from 799 to 735 to 707. In contrast, the number of unique formulas increased significantly from 461 to 498 to 622 showing a significant increment in the molecular diversity and variability for CHNO compounds along the light exposure continuum. In the case of CHOS compounds, the shared formulas with t=0 changed by decreasing from 212 to 198 to 151, while the unique formulas changed up from 124 to 166 and back down to 144. The commonality between both the O, N, S-functionalized CHNO and CHOS molecular members is that both increase their molecular complexity with increasing light exposure, with S inclined to a slight decrease at t=13 compared to t=6, but still larger compared to t=3. As such, photochemical processes may contribute substantially to the observed molecular diversity of heteroatom DOM in natural systems.

The data presented in Table S4 and corresponding Fig. S12, are intended to show the trends in molecular change along the light-exposure time series for total assigned members of the CHO, CHNO, and CHOS molecular series. Fig. S4A presents data of unique and shared compounds between specific pairs of light exposed samples (e.g. between t = 0 and t = 03; or between t = 6 and t = 13). While the number of shared compounds between time series pairs increased slightly for the intermediate time series experiments, the overall increment for the experimental endmembers was not particularly large (2377 to 2401). In contrast, the changes observed for the unique compounds shared between the pairs were more significant, with the number of shared components between t=3 and t=0 and between t = 6 and t = 13 being highest (916 and 818 respectively). Table S4 also presents the shared and unique CHNO and CHOS compounds between each pair in the light exposure series. While some heteroatom compounds seem to be relatively stable and partially shared along the light exposure continuum, a variety of compounds are also photoproduced or photo-consumed at each step. While both increases and decreases are observed throughout the pairs and no general trend could be observed, the fact that each time series had a significant number of unique heteroatom components compared to the prior and to the following exposure time suggests that the biogeochemistry of heteroatom DOM component is quite complex and the photochemical mechanisms controlling the molecular changes need to be investigated in detail. Further investigations on this subject should include the variations in photo-induced composition of heteroatom-DOM along the MW continuum.

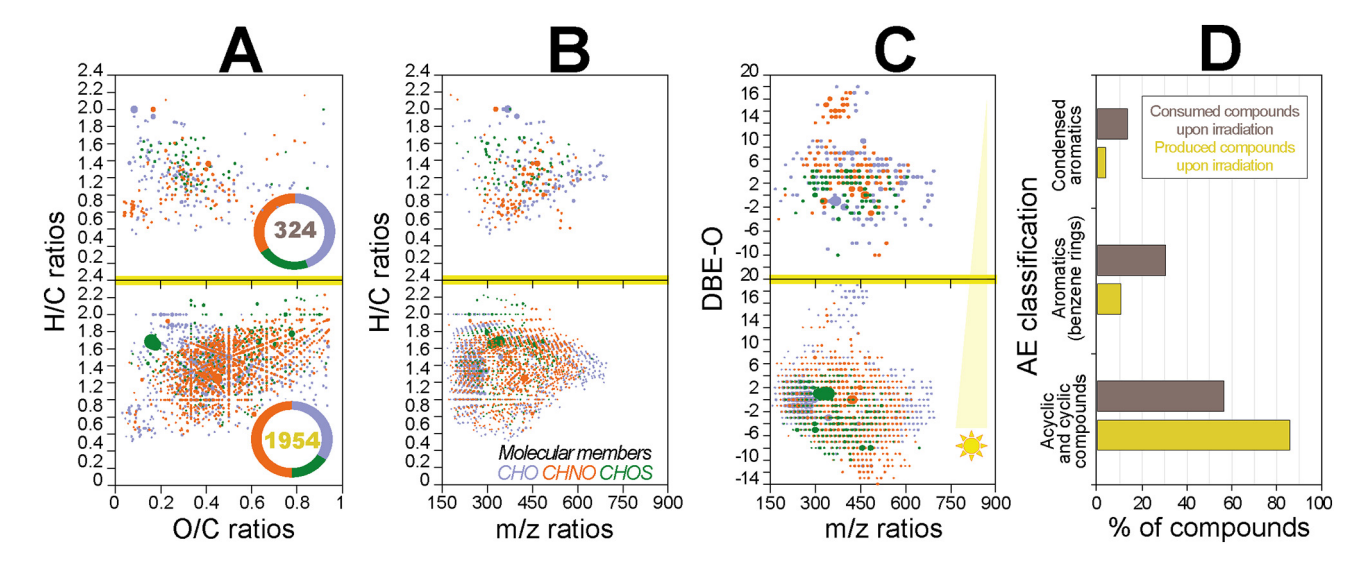


Fig. 6. Comparative assessment of the negative electrospray 12 T FT-ICR mass spectra: (top panel) consumed and (bottom panel) produced molecular compositions observed in all post-irradiation experiments. Color code according to CHO (blue), CHOS (green) and CHNO (orange) molecular series. Bubble areas reflect the relative and averaged abundance of respective compositions for the consumed and produced compounds, respectively. (panel A) van Krevelen diagrams. (panel B) mass-edited H/C elemental ratios. (panel C) Profile of unsaturation level of the molecular series. (panel D) computed percentage of variance for condensed aromatics, aromatics (benzene rings) as well as alicyclic and acyclic compounds using aromaticity equivalents (AI) (Yassine et al., 2014).

4. Conclusion

This study demonstrates a large diversity of heteroatom-dependent photochemistry of DOM which will affect the speciation of heteroatoms N and S and their biogeochemical linkages to inorganic species like ammonium anion (NH₄⁺), nitrite (NO₂⁻), nitrate (NO₃⁻) and $S_nO_m^{2-}$ (n: 1 or 2; m: 3 or 4). Photo-exposure of this DOM sample resulted in degradation, with release of small endmember molecules, as well as synthesis of oxygenated compounds, probably by secondary oxidation of reactive (radical) intermediates. The temporal evolution of photoproducts was non-linear and initial depletion of chromophores which often carried major unsaturation, was followed by a relative increase in oxygenated aliphatic compounds. The temporal evolution of CHOS compounds likely comprised photogeneration of oxidized sulfur-containing functional groups some of which decomposed on longer time scales or were transformed into FTMS-invisible compounds. CHO and oxygenated CHOS compounds were structurally more related than CHO and CHNO compounds likely as a consequence that oxygenated sulfur containing functional groups are attachment units C-O-S_nO_mH, and their alterations do not compromise the core structure of DOM whereas structural nitrogen is integrated into the DOM molecular skeleton. The higher apparent light-induced generation and photostability of CHNO compounds compared with CHO and CHOS compounds possibly reflects incorporation of structural nitrogen into DOM molecules. Photochemical transformations of DON have previously been reported in this ecosystem (Pisani et al., 2017). In that study, the DON reactivity in the Caloosahatchee River (northern Everglades) revealed that while the mean bioavailable DON (BDON) was about 15% (ranged from 12 to 61%) the effects of photo-exposure prior to bio-incubation did not have a significant effect on the %BDON. As such, it remains unknown at this point if the N-incorporation observed for the Hillsboro Canal DOM sample enhances or reduces the bioavailability of nitrogen in this coastal wetland. Remarkably, considerable resynthesis of olefins occurred during photo-exposure whereas oxygenated aromatic compounds were continually depleted, and carboxylated and alkylated benzene derivatives evolved non-uniformly. In addition to the photoproduction of low molecular weight CHO and CHNO compounds (≤450 Da) with high O/C ratios, higher numbers, and relative proportions of CHNO (50%) and CHOS (16%) than CHO (34%) compounds were photo-synthesized.

Overall, this study shows that light-induced changes in DOM can have a significant effect on heteroatom DOM molecular complexity, potentially leading to the generation of CHNO and CHOS compounds that are more water soluble and potentially more bioavailable. Such effects will be critical in the biogeochemical assessment of the potential implications of N and S on aquatic ecosystems affected by land-use changes and other anthropogenic influences (Roebuck et al., 2020). In the case of the Everglades ecosystem, both degradation and generation of CHNO and CHOS molecules were observed on time scales similar to the water residence time in this coastal wetland. As Everglades restoration efforts advance and enhanced water delivery is implemented, reducing the residence time of DOM in the system, some of the observed heteroatom DOM transformations may become limited, or transferred to more coastal waters. DOM in tributaries with elevated CDOM or high turbidity, might be initially shielded from such light-induced compositional changes, but as light availability increases due to dilution or sedimentation, these photochemical processes might become dominant in controlling the biogeochemical fate of CHNO and CHOS.

CRediT authorship contribution statement

Mourad Harir: FT-ICR/MS, writing - review & editing. Kaelin M. Cawley: Sampling, SEC, optical properties, writing - review & editing. Norbert Hertkorn: NMR data generation, writing - review & editing. Philippe Schmitt-Kopplin: Writing - review & editing. Rudolf Jaffé:

Sampling writing - review & editing. All the authors participate in the conceptualization and in the writing - original draft.

Declaration of competing interest

The authors declare that they have no known competing financial interests or personal relationships that could have appeared to influence the work reported in this paper.

Acknowledgments

This work was in part supported by the National Science Foundation through the Florida Coastal Everglades Long-Term Ecological Research program under Grant No. DEB-1237517 and the George Barley Endowment to RJ. The authors are also grateful to the FCE LTER support that has enabled the collaboration between SERC/Department of Chemistry and Biochemistry, and Helmholtz Munich, Research Unit Analytical Biogeochemistry (BGC)

Appendix A. Supplementary data

Supplementary data to this article can be found online at https://doi.org/10.1016/j.scitotenv.2022.155790.

References

- Amon, R.M.W., Fitznar, H.P., Benner, R., 2001. Linkages among the bioreactivity, chemical composition, and diagenetic state of marine dissolved organic matter. Limnol. Oceanogr. 46. 287–297.
- Balcarczyk, K., Jones Jr., J.B., Jaffé, R., Maie, N., 2009. Dissolved organic matter bioavailability and composition in streams draining catchments with discontinuous permafrost. Biogeochemistry 94, 255–270.
- Benner, R., Kaiser, K., 2011. Biological and photochemical transformations of amino acids and lignin phenols in riverine dissolved organic matter. Biogeochemistry. 102, 209–222.
- Berman, T., Bronk, D.A., 2003. Dissolved organic nitrogen: a dynamic participant in aquatic ecosystems. Aquat. Microb. Ecol. 31, 279–305.
- Bro, R., 1997. PARAFAC. Tutorial and applications. Chemom. Intell. Lab. Syst. 38, 149–171.
 Bushaw, K.L., Zepp, R.G., Tarr, M.A., SchulzJander, D., Bourbonniere, R.A., Hodson, R.E.,
 Miller, W.L., Bronk, D.A., Moran, M.A., 1996. Photochemical release of biologically available nitrogen from aquatic dissolved organic matter. Nature 381 (6581), 404–407.
- Chen, M., Jaffé, R., 2014. Photo- and bio-reactivity patterns of dissolved organic matter from biomass and soil leachates and surface waters in a subtropical wetland. Water Res. 61, 181–190.
- Chen, M., Price, R.M., Yamashita, Y., Jaffé, R., 2010. Comparative study of dissolved organic matter from groundwater and surface water in the Florida coastal Everglades using multidimensional spectrofluorometry combined with multivariate statistics. Appl. Geochem. 25, 872–880.
- Chen, M., Maie, N., Parish, K., Jaffé, R., 2013. Spatial and temporal variability of dissolved organic matter quantity and composition in an oligotrophic subtropical coastal wetland. Biogeochemistry 115, 167–183.
- Chin, W.C., Orellana, M.V., Verdugo, P., 1998. Spontaneous assembly of marine dissolved organic matter into polymer gels. Nature 391, 568–572.
- Coble, P.G., Schultz, C.A., Mopper, K., 1993. Fluorescence contouring analysis of DOC intercalibration experiment samples - a comparison of techniques. Mar. Chem. 41, 173–178.Derenne, S., 2001. A review of some important families of refractory macromolecules: composition, origin, and fate in soils and sediments. Soil. Sci. 166, 833–847.
- Derenne, S., Coelho, C., Anquetil, C., Szopa, C., Rahman, A.S., McMillan, P.F., Corà, F., Pickard, C.J., Quirico, E., Bonhomme, C., 2012. New insights into the structure and chemistry of Titan's tholins via 13C and 15N solid state nuclear magnetic resonance spectroscopy. Icarus 221, 844–853.
- Ding, Y., Watanabe, A., Jaffé, R., 2014. Dissolved black nitrogen (DBN) in freshwater environments: source and land to ocean flux assessment. Org. Geochem. 68, 1–4.
- Dittmar, T., Fitznar, H.P., Kattner, G., 2001. Origin and biogeochemical cycling of organic nitrogen in the eastern Arctic Ocean as evident from D- and L-amino acids. Geochim. Cosmochim. Acta 65. 4103–4114.
- Doane, T.A., 2017a. The abiotic nitrogen cycle. Acs. Earth. Space. Chem. 1 (7), 411–421.
- Doane, T.A., 2017b. A survey of photogeochemistry. Geochem. Trans. 1, 18.
- Fasnacht, M.P., Blough, N.V., 2002. Aqueous photodegradation of polycyclic aromatic hydrocarbons. Environ. Sci. Technol. 36, 4364–4369.
- Frankovich, T.A., Rudnick, D.T., Fourqurean, J.W., 2017. Light attenuation in estuarine mangrove lakes. Estuar. Coast. Shelf Sci. 184, 191–201.
- Gharehveran, M.M., Hain, E., Blaney, L., Shah, A.D., 2020. Influence of dissolved organic matter on carbonyl sulfide and carbon disulfide formation from cysteine during sunlight photolysis. Environ. Sci. Process. Impacts. 22, 1852.
- Glrigorovski, S., Strekowski, R., Barbati, S., Vione, D., 2015. Environmental implications of hydroxyl radicals (*OH). Chem. Rev. 115, 13051–13092.

- Gomez-Saez, G.V., Pohlabeln, A.M., Stubbins, A., Marsay, C.M., Dittmar, T., 2017. Photochemical alteration of dissolved organic sulfur from sulfidic porewater. Environ. Sci. Technol. 51, 14144–14154.
- Gonsior, M., Peake, B.M., Cooper, W.T., Podgorski, D., D'Andrilli, J., Cooper, W.J., 2009. Photochemically induced changes in dissolved organic matter identified by ultrahigh resolution fourier transform ion cyclotron resonance mass spectrometry. Environ. Sci. Technol. 43. 698–703.
- Gonsior, M., Hertkorn, N., Conte, M.H., Cooper, W.J., Bastviken, D., Druffel, E., Schmitt-Kopplin, P., 2014. Photochemical production of polyols arising from significant phototransformation of dissolved organic matter in the oligotrophic ocean. Mar. Chem. 163, 10–18.
- Gonsior, M., Luek, J., Schmitt-Kopplin, P., Grebmeier, J.M., Cooper, L.W., 2017. Optical properties and molecular diversity of dissolved organic matter in the Bering Strait and Chukchi Sea. Deep-Sea Res. II Top. Stud. Oceanogr. 144, 104–111.
- Gonsior, M., Hertkorn, N., Hinman, N., Dvorski, S.E.-M., Harir, M., Cooper, W.J., Schmitt-Kopplin, P., 2018. Yellowstone Hot Springs are organic chemodiversity hot spots. Sci. Rep. 8 (1) 14155
- Gonsior, M., Zwartjes, M.Z., Cooper, W.J., Ishida, K.P., Tseng, L.Y., Jeung, M.K., Rosso, D., Hertkorn, N., Schmitt-Kopplin, P., 2011. Molecular characterization of effluent organic matter identified by ultrahigh resolution mass spectrometry. Water Res. 45, 2943–2953.
- Hawkes, J.A., Radoman, N., Bergquist, J., Wallin, M.B., Tranvik, L.J., Löfgren, S., 2018. Regional diversity of complex dissolved organic matter across forested hemiboreal headwater streams. Sci. Rep. 8, 16060.
- Hertkorn, N., Benner, R., Frommberger, M., Schmitt-Kopplin, P., Witt, M., Kaiser, K., Kettrup, A., Hedges, J.I., 2006. Characterization of a major refractory component of marine dissolved organic matter. Geochim. Cosmochim. Acta. 70, 2990–3010.
- Hertkorn, N., Harir, M., Cawley, K.M., Schmitt-Kopplin, P., Jaffé, R., 2016. Molecular characterization of dissolved organic matter from subtropical wetlands: a comparative study through the analysis of optical properties, NMR and FTICR/MS. Biogeosciences 13. 1–21.
- Herzsprung, P., Hertkom, N., Friese, K., Schmitt-Kopplin, P., 2010. Photochemical degradation of natural organic sulfurcompounds (CHOS) from iron-rich mine pit lake porewaters an initial understanding from evaluation of single-elemental formulae using ultra-high-resolutionmass spectrometry. Rapid Commun. Mass Spectrom. 24, 2909–2924.
- Herzsprung, P., Hertkorn, N., von Tumpling, W., Harir, M., Friese, K., Schmitt-Kopplin, P., 2016. Molecular formula assignment for dissolved organic matter (DOM) using high-field FT-ICR-MS: chemical perspective and validation of Sulphur-rich organic components (CHOS) in pit lake samples. Anal. Bioanal. Chem. 408, 2461–2469.
- Hjerrilg, P., Torring, T., Poulsen, T.B., 2020. Dehydration reactions in polyfunctional natural products. Nat. Prod. Rep. 37, 1043–1064.
- Jaffé, R., McKnight, D., Maie, N., Cory, R., McDowell, W.H., Campbell, J.L., 2008. Spatial and temporal variations in DOM composition in ecosystems: the importance of long-term monitoring of optical properties. J. Geophys. Res. Biogeosci. 113, G04032.
- Kaiser, E., Sulzberger, B., 2004. Phototransformation of riverine dissolved organic matter (DOM) in the presence of abundant iron: effect on DOM bioavailability. Limnol. Oceanogr. 49, 540–554.
- Kamjunke, N., Hertkorn, N., Harir, M., Schmitt-Kopplin, P., Griebler, C., Brauns, M., von Tümpling, W., Weitere, M., Herzsprung, P., 2019. Molecular change of dissolved organic matter and patterns of bacterial activity in a stream along a land-use gradient. Water Res. 164, 114919.
- Kang, P.-G., Mitchel, M.J., 2013. Bioavailability and size-fraction of dissolved organic carbon, nitrogen, and sulfur at the arbutus lake watershed, Adirondack Mountains, NY. Biogeochemistry 115, 213–234.
- Ksionzek, K.B., Lechtenfeld, O.J., McCallister, S.L., Schmitt-Kopplin, P., Geuer, J.K., Geibert, W., et al., 2016. Dissolved organic sulfur in the ocean: biogeochemistry of a petagram inventory. Science 354, 456–459.
- Kujawinski, E.B., Del Vecchio, R., Blough, N.V., Klein, G.C., Marshall, A.G., 2004. Probing molecular-level transformations of dissolved organic matter: insights on photochemical degradation and protozoan modification of DOM from electrospray ionization fourier transform ion cyclotron resonance mass spectrometry. Mar. Chem. 92, 23–37.
- Levine, N.M., 2016. Putting the spotlight on organic sulfur. Science 354, 418–419.
- Levine, N.M., Toole, D.A., Neeley, A., Bates, N.R., Doney, S.C., Dacey, J.W.H., 2016. Revising upper-ocean sulfurdynamics near Bermuda: New lessons from 3 years of con-centration and rate measurements. Environ. Chem. 13, 302–313.
- Leyva, D., Tose, L.V., Porter, J., Wolff, J., Jaffé, R., Fernandez-Lima, F., 2019. Understanding the structural complexity of dissolved organic matter: isomeric diversity. Faraday Discuss. 218, 431.
- Lundeen, R.A., Janssen, E.M.L., Chu, C.H., McNeill, K., 2014. Environmental photochemistry of amino acids, peptides and proteins. Chimia 68 (11), 812–817.
- Maie, N., Scully, N.M., Pisani, O., Jaffé, R., 2007. Composition of a protein-like fluorophore of dissolved organic matter in coastal wetland and estuarine ecosystems. Water Res. 41, 563-570
- Mao, R., Li, S.Y., 2019. Temporal controls on dissolved organic carbon biodegradation in subtropical rivers: initial chemical composition versus stoichiometry. Sci. Total Environ. 651, 3064–3069
- Margolin, A.R., Gonnelli, M., Hansell, D.A., Santinelli, C., 2018. Black Sea dissolved organic matter dynamics: insights from optical analyses. Limnol. Oceanogr. 63, 1425–1443.
- McCarthy, M.D., Benner, R., Lee, C., Hedges, J.I., Fogel, M.L., 2004. Amino acid carbon isotopic fractionation patterns in oceanic dissolved organic matter: an unaltered photoautotrophic source for dissolved organic nitrogen in the ocean? Mar. Chem. 92, 123–134.
- Mckay, G., Huang, W., Romera-Castillo, C., Crouch, J., Rosario-Ortiz, F.L., Jaffé, R., 2017.
 Assessing dissolved organic matter photo-reactivity in a subtropical wetland ecosystem: correlations between optical properties, antioxidant capacity, and the photochemical formation of reactive intermediates. Environ. Sci. Technol. 51, 5404–5413.

- McKnight, D.M., Aiken, G.R., 1998. Sources and age of aquatic humus. In: Hessen, D.O., Tranvik, L.J. (Eds.), Ecological Studies. Springer-Verlag, Berlin Heidelberg Inc., New York, pp. 9–39 133.
- McKnight, D.M., Boyer, E.W., Westerhoff, P.K., Doran, P.T., Kulbe, T., Andersen, D.T., 2001. Spectrofluorometric characterization of dissolved organic matter for indication of precursor organic material and aromaticity. Limnol. Oceanogr. 46, 38–48.
- McVoy, C.W., Said, W.P., Obeysekera, J., Van Arman, J., Dreschel, T., 2011. Landscapes and Hydrology of the Pre-drainage Everglades. University Press of Florida, Gainesville, FL.
- Medeiros, P.M., Seidel, M., Powers, L.C., Dittmar, T., Hansell, D.A., Miller, W.L., 2015. Dissolved organic matter composition and photochemical transformations in the northern North Pacific Ocean. Geophys. Res. Lett. 42, 863–870.
- Mesfioui, R., Abdulla, H.A.N., Hatcher, P.G., 2015. Photochemical alterations of natural and anthropogenic dissolved organic nitrogen in the York River. Environ. Sci. Technol. 49, 159–167.
- Mopper, K., Zhou, X., 1990. Hydroxyl radical photoproduction in the sea and its potential impact on marine processes. Science 250 (4981), 661.
- Niu, X.-Z., Croué, J.-P., 2019. Photochemical production of hydroxyl radical from algal organic matter. Water Res. 161, 11–16.
- Niu, X.Z., Busetti, F., Langsa, M., Croue, J.P., 2016. Roles of singlet oxygen and dissolved organic matter in self-sensitized photo-oxidation of antibiotic norfloxacin under sunlight irradiation. Water Res. 106, 214–222.
- Niu, X.-Z., Harir, M., Schmitt-Kopplin, P., Croué, J.P., 2019. Sunlight-induced phototransformation of transphilic and hydrophobic fractions of Suwannee River dissolved organic matter. Sci. Total Envirop. 694, 133737.
- Ohno, T., 2002. Fluorescence inner-filtering correction for determining the humification index of dissolved organic matter. Environ. Sci. Technol. 36, 742–746.
- Opsahl, S., Benner, R., 1998. Photochemical reactivity of dissolved lignin in river and ocean waters. Limnol. Oceanogr. 43, 1297–1304.
- Ossola, R., Tolu, J., Clerc, B., Erickson, P.R., Winkel, L.H.E., McNeill, K., 2019. Photochemical production of sulfate and methanesulfonic acid from dissolved organic sulfur. Environ. Sci. Technol. 53, 13191–13200.
- Osterholz, H., Singer, G., Wemheuer, B., Daniel, R., Simon, M., Niggemann, J., Dittmar, T., 2016. Deciphering associations between dissolved organic molecules and bacterial communities in a pelagic marine system. ISME 10, 1717–1730.
- Pattison, D.I., Rahmanto, A.S., Davies, M.J., 2012. Photo-oxidation of proteins. Photochem. Photobiol. Sci. 11 (1), 38–53.
- Pisani, O., Boyer, J.N., Podorski, D.C., Thomas, C.R., Coley, T., Jaffé, R., 2017. Molecular composition and bioavailability of dissolved organic nitrogen in a lake flow-dominated river in south Florida, USA. Aquat. Sci. 79 (4), 891–908.
- Pohlabeln, A.M., Gomez-Saez, G.V., Noriega-Ortega, B.E., Dittmar, T., 2017. Experimental evidence for abiotic sulfurization of marine dissolved organic matter. Front. Mar. Sci. 4, 364
- Remucal, C.K., McNeill, K., 2011. Photosensitized amino acid degradation in the presence of riboflavin and its derivatives. Environ. Sci. Technol. 45 (12), 5230–5237.
- Rodriguez-Zuniga, U.F., Milori, D.M.B.P., da Silva, W.T.L., Martin-Neto, L., Oliveria, L.C., Rocha, J.C., 2008. Changes in optical properties caused by UV-irradiation of aquatic humic substances from the Amazon River basin: seasonal variability evaluation. Environ. Sci. Technol. 42, 1948–1953.
- Roebuck, J.A., Seidel, M., Dittmar, T., Jaffé, R., 2018. Land use controls on the spatial variability of dissolved black carbon in a subtropical watershed. Environ. Sci. Technol. 52, 8104–8114.
- Roebuck Jr., J.A., Seidel, M., Dittmar, T., Jaffé, R., 2020. Controls of land use and the river continuum concept on dissolved organic matter composition in an anthropogenically disturbed subtropical watershed. Environ. Sci. Technol. 54, 195–206.
- Roger, A., Sallet, D., Lemaire, J., 1986. Photochemistry of aliphatic polyamides. 4. Mechanisms of photooxidation of polyamides 6, 11, and 12 at long wavelengths. Macromolecules 19, 579–584.
- Schmitt-Kopplin, P., Hertkom, N., Schulten, H.R., Kettrup, A., 1998. Structural changes in a dissolved soil humic acid during photochemical degradation processes under O-2 and N-2 atmosphere. Environ. Sci. Technol. 32, 2531–2541.
- Seidel, M., Beck, M., Riedel, T., Waska, H., Suryaputra, I.G.N.A., Schnetger, B., et al., 2014. Biogeochemistry of dissolved organic matter in an anoxic intertidal creek bank. Geochim. Cosmochim. Acta 140, 418–434.
- Seidel, M., Manecki, M., Herlemann, D.P.R., Deutsch, B., Schulz-Bull, D., Jürgens, K., Dittmar, T., 2017. Composition and transformation of dissolved organic matter in the Baltic Sea. Front. Earth Sci. 5, id.31.
- Sharpless, C.M., Aeschbacher, M., Page, S.E., Wenk, J., Sander, M., McNeill, K.J., 2014. Photooxidation-induced changes in optical, electrochemical, and photochemical properties of humic substances. Envir. Sci. Technol. 48 (5), 2688–2696.
- Sleighter, R., Hatcher, P.G., 2008. Molecular characterization of dissolved organic matter (DOM) along a river to ocean transect of the lower Chesapeake Bay by ultrahigh resolution electrospray ionization fourier transform ion cyclotron resonance mass spectrometry. Mar. Chem. 110, 140–152.
- Sleighter, R.L., Lie, Z.F., Xue, J.H., Hatcher, P.G., 2010. Multivariate statistical approaches for the characterization of dissolved organic matter analyzed by ultrahigh resolution mass spectrometry. Environ. Sci. Technol. 44, 7576–7582.
- Stedmon, C.A., Bro, R., 2008. Characterizing dissolved organic matter fluorescence with parallel factor analysis: a tutorial. Limnol. Oceanogr. Methods 6, 572–579.
- Stubbins, A., Dittmar, T., 2015. Illuminating the deep: molecular signatures of photochemical alteration of dissolved organic matter from North Atlantic deep water. Mar. Chem. 177. Part 2. 318–324.
- Stubbins, A., Spencer, R.G.M., Chen, H., Hatcher, P.G., Mopper, K., Hernes, P.J., Mwamba, V.L., Mangangu, A.M., Wabakanghanzi, J.N., Six, J., 2010. Illuminated darkness: molecular signatures of Congo River dissolved organic matter and its photochemical alteration as revealed by ultrahigh precision mass spectrometry. Limnol. Oceanogr. 55, 1467–1477.

- Tarr, M., Wang, W., Bianchi, T.S., Engelhaupt, E., 2001. Mechanisms of ammonia and amino acid photoproduction from aquatic humic and colloidal matter. Water Res. 35, 3688–3696
- Thorp, J.H., Delong, M.D., 2002. Dominance of autochthonous autotrophic carbon in food webs of heterotrophic rivers. Oikos 96, 543–550.
- Tominta, M., Masachika, I., Ukita, T., 1969. Sensitized photooxidation of histidine and its derivatives. Products and mechanisms of the reaction. Biochemistry 8 (12), 5149–5160.
- Tremblay, L.B., Dittmar, T., Marshall, A.G., Cooper, W.J., Cooper, W.T., 2007. Molecular characterization of dissolved organic matter in a north brazilian mangrove porewater and mangrovefringed estuaries by ultrahigh resolution fourier TransformIon cyclotron resonance mass spectrometry and excitation/emission spectroscopy. Mar. Chem. 105, 15–29.
- Tziotis, D., Hertkorn, N., Schmitt-Kopplin, P., 2011. Kendrickanalogous network visualisation of ion cyclotron resonance fourier transform mass spectra: improved options for the assignment of elemental compositions and the classification of organic molecular complexity. Eur. Mass. Spectrom. 17, 415–421.
- Vähätalo, A.V., 2009. Light, photolytic productivity and chemical products. In: Likens G (ed) Encyclopedia of inland waters. Elsevier, Oxford. 2, 761–773.
- Vähätalo, A.V., Zepp, R.G., 2005. Photochemical mineralization of dissolved organic nitrogen to ammonium in the Baltic Sea. Environ. Sci. Technol. 39 (18), 6985–6992.
- Valle, J., Harir, M., Gonsior, M., Enrich-Prast, A., Schmitt-Kopplin, P., Bastviken, D., Hertkorn, N., 2020. Molecular differences between water column and sediment pore water SPE-DOM in ten swedish boreal lakes. Water Research. Water. Res. 170, 115320.
- Waggoner, D.C., Wozniak, A.S., Cory, R.M., Hatcher, P.G., 2017. The role of reactive oxygen species in the degradation of lignin derived dissolved organic matter. Geochim. Cosmochim. Acta 208, 171–184.
- Wagner, S., Jaffé, R., 2015. Effects of photodegradation on molecular size distribution and quality of dissolved black carbon. Org. Geochem. 86, 1–4.
- Wagner, S., Dittmar, T., Jaffé, R., 2015a. Molecular characterization of dissolved black nitrogen by electrospray ionization fourier transform ion cyclotron resonance mass spectrometry. Org. Geochem. 79, 21–30.

- Wagner, S., Riedel, T., Niggemann, J., Vahatalo, A., Dittmar, T., Jaffé, R., 2015b. Linking the molecular signature of heteroatomic dissolved organic matter to watershed characteristics in world Rivers. Environ. Sci. Technol. 49, 13798–13806.
- Ward, C.P., Cory, R.M., 2016. Complete and partial photo-oxidation of dissolved organic matter draining permafrost soils. Environ. Sci. Technol. 50, 3545–3553.
- Watanabe, A., Tsutsuki, K., Inoue, Y., Maie, N., Melling, L., Jaffé, R., 2014. Composition of dissolved organic nitrogen in rivers associated with wetlands. Sci. Total Environ. 493, 220–228.
- Watts, Z.I., Easton, C.J., 2009. Peculiar stability of amino acids and peptides from a radical perspective. J. Am. Chem. Soc. 131, 11323–11325.
- Weishaar, J.L., Aiken, G.R., Bergamaschi, B.A., Fram, M.S., Fujii, R., Mopper, K., 2003. Evaluation of specific ultraviolet absorbance as an indicator of the chemical composition and reactivity of dissolved organic carbon. Environ. Sci. Technol. 37, 4702–4708.
- Wetzel, R.G., Hatcher, P.G., Bianchi, T., 1995. Natural photolysis by ultraviolet irradiance of recalcitrant organic matter to simple substrates for rapid bacterial metabolism. Limnol. Oceanogr. 40 (89), 1369–1380.
- Yamashita, Y., Scinto, L.J., Maie, N., Jaffé, R., 2010. Dissolved organic matter characteristics across a subtropical Wetland's landscape: application of optical properties in the assessment of environmental dynamics. Ecosystems 13, 1006–1019.
- Yassine, M.M., Harir, M., Dabek-Zlotorzynska, E., Schmitt-Kopplin, P., 2014. Structural characterization of organic aerosol using fourier transform ion cyclotron resonance mass spectrometry: aromaticity equivalent approach. Rapid Commun. Mass Spectrom. 28, 2445–2454.
- Yu, Z., Zhang, Q., Kraus, T.E.C., Dahlgren, R.A., Anastasio, C., Zasoski, R.J., 2002. Contribution of amino compounds to dissolved organic nitrogen in forest soils. Biogeochemistry 61, 173–198.
- Zepp, R.G., Wolfe, N.L., Baughman, G., Hollis, R.C., 1977. Singlet oxygen in natural waters. Nature 267. 421–423.
- Zou, K., Thébault, E., Lacroix, G., Barot, S., 2015. Interactions between the green and brown food web determine ecosystem functioning. Funct. Ecol. 30, 1454–1465.